PCCP

Accepted Manuscript

ROYAL SOCIETY OF CHEMISTRY

www.rsc.org/pccp

PCCP Physical Chemistry Chemical Physics Dynamic Article Links ►

Cite this: DOI: 10.1039/c0xx00000x

www.rsc.org/xxxxxx

ARTICLE TYPE

Effects of 3d transition-metal doping on electronic and magnetic properties of MoS_2 nanoribbons

Xiaoqing Tian,[a] Lin Liu,[a] Yu Du,*[a] Juan Gu,[a] Jian-bin Xu,[c] and Boris I. Yakobson*[b]

Received (in XXX, XXX) Xth XXXXXXXXX 20XX, Accepted Xth XXXXXXXXX 20XX

DOI: 10.1039/b000000x

The electronic and magnetic properties of MoS_2 nanoribbons doped with 3d transitional metals (TMs) were investigated using first-principles calculations. Clean armchair MoS_2 nanoribbons ($AMoS_2NRs$) are nonmagnetic semiconductors whereas clean zigzag MoS_2 nanoribbons ($ZMoS_2NRs$) are metallic magnets. The 3d TM impurities tend to substitute the outermost cations of $AMoS_2NRs$ and $ZMoS_2NRs$, which are in agreement with the experimental results reported. The magnetization of the 3d-TM-impurity-doped $AMoS_2NRs$ and $ZMoS_2NRs$ is configuration dependent. The band gap and carrier concentration of $AMoS_2NRs$ can be tuned by 3d-TM doping. Fedoped $AMoS_2NRs$ exhibit ferromagnetic characteristics and the Curie temperature (T_C) can be tuned using different impurity concentrations. Co-doped $ZMoS_2NRs$ are strongly ferromagnetic with a T_C above room temperature.

Introduction

The MoS_2 monolayer is composed of three covalently bonded hexagonal atomic layers (S–Mo–S). Weak van der Waals interactions exist between adjacent MoS_2 monolayers. One important advantage of MoS_2 is that the electronic and optical properties can be tuned by varying the number of layers. The bulk MoS_2 crystal is an indirect gap semiconductor with a band gap of 1.29 eV, whereas the MoS_2 monolayer layer is a direct gap semiconductor with a band gap of 1.90 eV.[1,2] One-dimensional MoS_2 has been synthesized in recent experiments.[3,4] Quasi-1D nanotubes and nanoribbons of MoS_2 share the honeycomb structure and are expected to display interesting electronic and magnetic properties arising from quantum confinement effects.[5,6] Defects and strain are expected to modify the electronic properties and magnetic of MoS_2 monolayer and nanoribbons.[7–10] MoS_2 nanostructures are doped with 3d TMs such as Fe, Co, and Ni to increase its catalytic activities in hydrodesulfurization processes in the oil industry.[11,12] The magnetic and electronic properties of MoS_2 nanoribbons could be tuned by 3d TMs doping. Either 3d TM substrates or 3d TM nanoclusters could alter the electronic structures of MoS_2 monolayer.[13,14] We used state-of-the-art first-principles technique to study the electronic and magnetic properties of 3d TMs (including Mn, Fe, and Co)-doped MoS_2 nanoribbons with armchair- and zigzag-shaped edges.

Computational methods

Theoretical calculations were performed with the Quantum Espresso package,[15] employing the GGA-PBE exchange correlation functional.[16] The on-site Coulomb interaction GGA+U for 3d TMs is used.[17] The U and J are the on-site Coulomb repulsion and exchange interaction parameters, respectively. Typical values of U and J are 4.0 and 1.0 eV, respectively, for both Mn and Fe;[18,19] for Co, U and J are 3.3 and 1.0 eV. 40 Ry is used as the plane-wave basis set cutoff. The structural models of MoS_2 nanoribbons are constructed by cutting a single-layered MoS_2 with the desired edges and widths. The 1-D periodic boundary condition was applied along the growth direction of the nanoribbons to simulate infinitely long nanoribbon systems; the length scales for the MoS_2 nanoribbons are defined in Ref. 5. Specifically, the width of $AMoS_2NRs$ is defined by the number of dimmer columns whereas for $ZMoS_2NRs$ it is defined by the number of Mo columns. A 1.6-nm-thick vacuum layer was used to eliminate longitudinal interactions between the super cells. For the 14-$AMoS_2NR$, the

super cell contains in total 168 atoms, and its in-plane size is around 3.5 nm (width)×2.2 nm, which is large enough to avoid lateral image interactions. For 10-ZMoS$_2$NR, the super cell contains in total 120 atoms, and its in-plane size is around 4.0 nm (width)×0.7 nm, which is also large enough to avoid lateral image interactions. A sampling of 12 uniformly distributed k-points along the 1-D Brillouin zone is employed for the MoS$_2$ nanoribbons for both the zigzag and armchair shaped edges.

Results and discussion

The structures of relaxed 14-AMoS$_2$NRs (Fig. 1(a)) give a width of around 2.1 nm. After structural optimization, the width of 14-AMoS$_2$NR is increased by around 1.5 percent. There is obvious structural reconstruction to mitigate the truncation of chemical bonds at the edges. The S–Mo bonds in MoS$_2$ are composed of partial covalent and ionic bonds similar to the bonds of ZnO. The oxidation state of the edgiest Mo is +1.63, which is 0.1 smaller than that of the interior Mo using the Bader analysis method.[20] The edgiest Mo atom is moved by 0.3 Å inwards relative to the edgiest S atom. The bond length of S–Mo bond is about 0.1 Å smaller than that of the interior bond. The calculated spin-polarized density of states (SPDOS) of 14-AMoS$_2$NR (Fig. 1(b)). The 14-AMoS$_2$NR is a nonmagnetic semiconductor with band gaps of 0.56 eV and this is in good agreement with Ref. 5. The band gap value is determined by the difference in the on-site energies of two edges, and intra- and inter-edge hopping parameters of the tight-binding models.[21] Because clean 14-AMoS$_2$NR is a nonmagnetic semiconductor, 3d TMs (Mn, Fe, Co) are used as dopants to achieve magnetic properties. Seven substitution sites are considered (Fig. 1(a)) with impurity concentrations corresponding to 1.79 percent. Substituted by 3d TMs, the 14-AMoS$_2$NRs with its seven sites give seven configurations. 3d TM-doped 14-AMoS$_2$NRs exhibit obvious configuration-dependent formation energies and electronic and magnetic properties. Their formation energies are calculated from

$$\Delta H_f(TM) = E_{tot}(TM) - E_{tot}(clean) - \sum_i n_i \mu_i , \qquad (1)$$

where $E_{tot}(TM)$ is the total energy of the doped 14-AMoS$_2$NR and $E_{tot}(TM)$ the total energy of the undoped 14-AMoS$_2$NR. μ_i denotes the chemical potential for species i (host atoms or dopants), and n_i the corresponding number that have been added to or removed from the supercell.

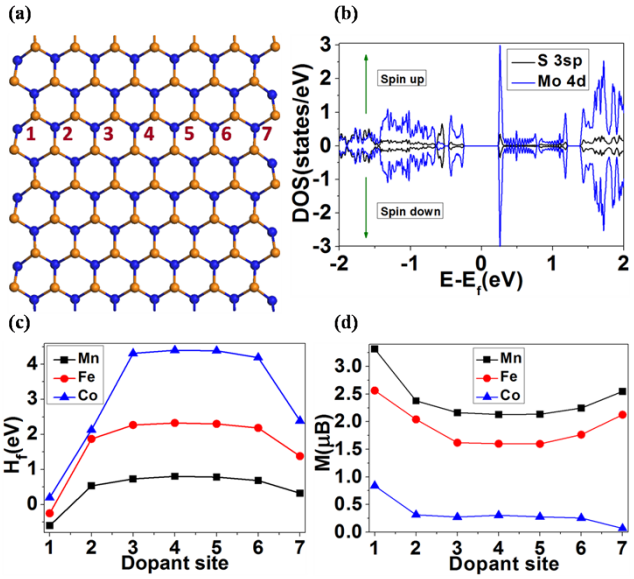

Fig. 1 (a) Top view of relaxed 14-AMoS$_2$NR and seven substitutional sites. (b) SPDOS of relaxed 14-AMoS$_2$NRs. (c) Formation energy of the 3d TM-doped 14-AMoS$_2$NRs for the seven configurations. (d) Configuration-dependent magnetic moment (M) of the 3d TM impurities in 14-AMoS$_2$NRs. 14-AMoS$_2$NRs are extended periodically along the *y* direction. Mo atoms are blue, S atoms are orange, and Fe atoms are red. For S and Mo, the SPDOS presented here is the averaged value of each atomic species (total SPDOS of S or Mo atoms divided by the number of atoms). This notion is used throughout the paper.

For 3d TM-doped 14-AMoS$_2$NR, configuration 1 has the lowest formation energy (Fig. 1(c)), and hence is the most favored. Configuration 4 has the highest formation energy, so is the least favored. The 3d TM impurities tend to replace the outermost cations. The order of the formation energies is H_f *(Mn)*< H_f *(Fe)* <H_f *(Co)*. This can be attributed to size effects of the 3d dopants; the larger the atomic radius of the dopant, the closer it is to the host Mo atom and thus the lower the formation energy. From the configuration-dependent magnetic moment of the 3d TM impurities (Fig. 1(d)), the magnetic moments of the impurities in configuration 1 for the 3d TM-impurity-doped 14-AMoS$_2$NRs, are larger than those of other configurations. Mn, Fe, and Co impurities of configuration 1 have local magnetic moments of 3.3, 2.5, and 0.9 Bohr magneton (μ_B), respectively. Similarly, Mn, Fe, and Co adatoms on the MoS$_2$ monolayer have local magnetic moments of 3.0, 2.0, and 1.0 μ_B, respectively.[22]

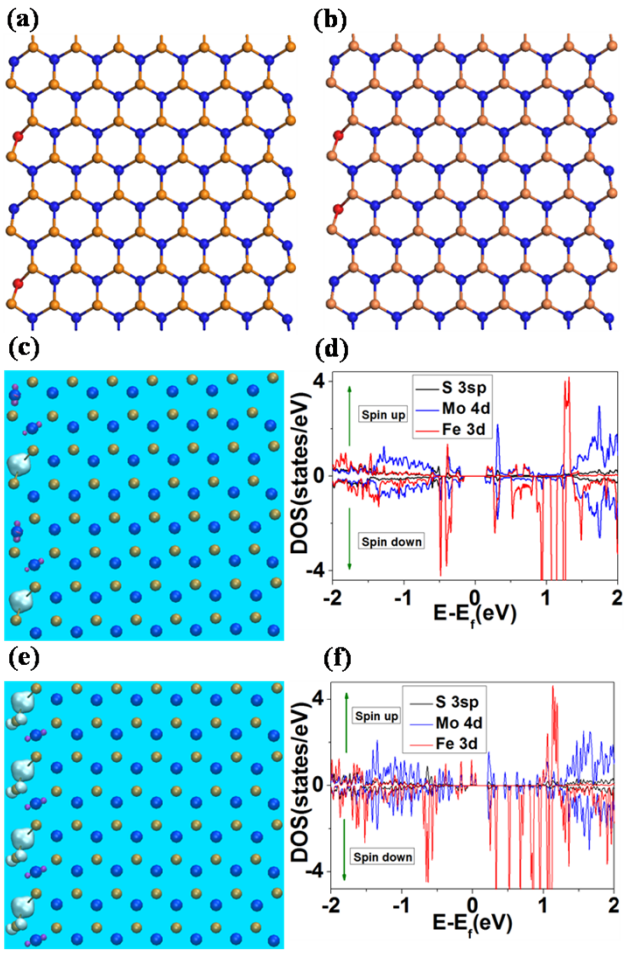

Fig. 2 Top views of the Fe-impurity-pair-doped 14-AMoS$_2$NR with configurations (a) α and (b) β. (c) 0.04 e/Å^3 isosurface and (d) SPDOS of the FM state of configuration α. (e) 0.04 e/Å^3 isosurface and (f) SPDOS of the FM state of Fe-doped 14-AMoS$_2$NR with a higher impurity concentration of 7.14 percent. For isosurfaces of the magnetization density distribution, white corresponds to a positive magnetization isosurface, and purple corresponds to a negative magnetization isosurface. This correspondence is used throughout the paper.

We further increase the concentration of 3d TM impurities to 3.57 percent to investigate the magnetic exchange interactions. For the configurations α and β for the optimized structures of Fe-impurity-pair-doped 14-AM$_O$S$_2$NRs (Fig. 2(a) and (b)), the Fe impurity pair are next-nearest-neighbors and nearest-neighbors along the edge. The total energy difference between the ferromagnetic (FM) and antiferromagnetic (AFM) states is defined as

$$\Delta E = E_{AF} - E_F \,, \tag{2}$$

where E_{AF} and E_{FM} are the total energies of the AFM and FM state, respectively. The ΔE is 21 meV for the Fe-impurity-pair-doped 14-AMoS$_2$NRs with configuration α, so the FM state is more stable than the AFM state. The magnetic exchange coupling of configuration β gave a ΔE of 11 meV which is 10 meV smaller than that of configuration α. There exists FM coupling between the Fe impurity pairs. We further increased the on-site Coulomb repulsion interaction U to 5 and 6 eV and found that ΔE was almost unchanged. The Ruderman–Kittel–Kasuya–Yosida interaction could be the origin of the ferromagnetism.[23] The magnetic exchange interactions between the 3d TM impurities in Heisenberg model[24] is written as:

$$H = -2JS_1 \cdot S_2 \,, \tag{3}$$

where J is the magnetic exchange coupling between neighboring magnetic atoms; S_1 and S_2 are the spins of the magnetic atoms 1 and 2. The total spin of the atom is given by $S = (N_\uparrow - N_\downarrow)/2$;[25] here $N_\uparrow$ and $N_\downarrow$ are the numbers of spin-up and spin-down electrons, respectively. According to eqns (2) and (3), the magnetic exchange coupling is obtained from $J = \Delta E/(4S_1 \cdot S_2)$. Here each Fe has a local magnetic moment of 2.5 μ_B. Thus we can take $S = S_1 = S_2 = 1.25$. Based on these values, the magnetic exchange coupling J is 3.36 meV for Fe-doped 14-AMoS$_2$NR with configuration α. The critical temperature T_C as estimated using the mean field method[26] is

$$T_C = \frac{2S(S+1)}{3k_B} J = \frac{(1+\frac{1}{S})\Delta E}{6k_B} \,, \tag{4}$$

Table 1 Summary of ΔE (meV) for 3d TM impurity-doped AMoS$_2$NRs of different widths. α and β refer to configurations α and β, respectively

	10_α	10_β	12_α	12_β	14_α	14_β	16_α	16_β
M n	−26	−13	−20	−16	−23	−14	−23	−18
Fe	30	10	15	8	21	11	22	13
Co	−4	−3	−3	−5	−5	−7	−6	−5

Here the calculated T_C is 73 K. From the magnetic exchange coupling for Fe-pair-doped AMoS$_2$NRs of different widths (see Table 1), ΔE is 30, 15, and 22 meV for the Fe-doped 10-, 12- and 16-AMoS$_2$NRs, respectively in configuration α giving a corresponding T_C of 104, 52, and 76 K calculated using eqn (4).

The ΔE is 10, 8, and 13 meV for the Fe-doped 10-, 12-, and 16-$AMoS_2$NRs, respectively, in configuration β giving a corresponding T_C of 35, 28, and 45 K. For these $AMoS_2$NRs, the T_C associated with configuration α is higher than that for configuration β. As indicated in Fig. 2(c), the magnetization of a doped 14-$AMoS_2$NR is mainly distributed on the Fe pair, and the Mo atoms along the doped edge have opposite magnetization directions to Fe. The edge states contribute mainly to the magnetization and occupy the electronic orbitals near the Fermi level. Thus the edge states are more active and dominate the physical properties of $AMoS_2$NRs. Compared with clean 14-$AMoS_2$NRs, the band gap of the Fe-pair-doped 14-$AMoS_2$NR has been obviously reduced. Based on Fig. 2(d), the band-gap values are 0.35 and 0.29 eV for the spin-up (majority) and spin-down (minority) bands, respectively. The blue shifts of the band gaps of 3d TM-doped $AMoS_2$NRs are expected to be observed in experiments. Similar band gap reduction effects were found in Cu-doped ZnO.[27] Hybridization of the Fe-impurity bands with MoS_2 raises up the valence band of the 14-$AMoS_2$NRs, which leads to a reduction in the band gap. Moreover, Fe ($3d^64s^2$) has more valence electrons than Mo ($4d^55s^1$), so it could inject excess electron carriers into MoS_2 and lead to N-type doping effects. Similarly, doping of the Co ($3d^74s^2$) and Mn ($3d^54s^2$) impurities will also turn MoS_2 into a N-type semiconductor. This is confirmed from results from density function theory indicating the Fermi level is raised by the doping of these 3d TM impurities. For doped 14-$AMoS_2$NRs, substitutions of Mn, Fe, and Co with a concentration of 3.57 percent will lift up the Fermi level by 0.09, 0.01, and 0.20 eV, respectively. This will enhance the local chemical affinity and reduce the work function of $AMoS_2$NRs.

Similarly, given the magnetic exchange couplings for the Mn and Co impurities in $AMoS_2$NRs (see Table 1), the values of all ΔE are negative, so the AFM state should be the ground state for Mn- and Co-doped $AMoS_2$NRs. The impurity concentration in 14-$AMoS_2$NRs is further increased to 7.14 percent (all Mo atoms of the left edge are substituted by Fe). The magnetization of this configuration (Fig. 2(e)) is mainly distributed on the Fe impurities, with the Mo atoms along the doped edge having opposite magnetization directions to Fe. ΔE was 278 meV for two Fe impurity pairs, so we should normalize the value of ΔE to 139 meV. The magnetic exchange coupling J is 22 meV calculated by $J=\Delta E/(4S_1 \cdot S_2)$ and the T_C is 481 K based on eqn (4). Thus the magnetic exchange coupling is enhanced by increasing the concentration of Fe impurities; the T_C of Fe-doped 14-$AMoS_2$NR is far above room temperature.

Based on the SPDOS (Fig. 2(f)), the band gap of spin-up and spin-down bands is 0.18 and 0.26 eV, respectively, so the band gap has been further reduced by increasing the concentration of Fe impurities.

The temperature-dependent magnetic moment can be estimated from the Stoner and spin-fluctuation models,[26]

$$M = M_0\left[1-(\frac{T}{T_c})^2\right]^{\frac{1}{2}}, \quad (5)$$

$$M = M_0\left[1-(\frac{T}{T_c})\right]^{\frac{1}{2}}, \quad (6)$$

where M_0 is the magnetization of the ground state. The M_0 of each Fe impurity of doped 14-$AMoS_2$NR, with structure shown in Fig. 2(e), is 2.5 μ_B. As the temperature increases, M decreases. At room temperature (300 K), the Stoner and spin-fluctuation models predict 1.9 and 1.5 μ_B, respectively for M. The Fe impurity still has a strong magnetic moment at room temperature because of the high T_C. This is very important for MoS_2 applications in spintronics and magnetic data storage.

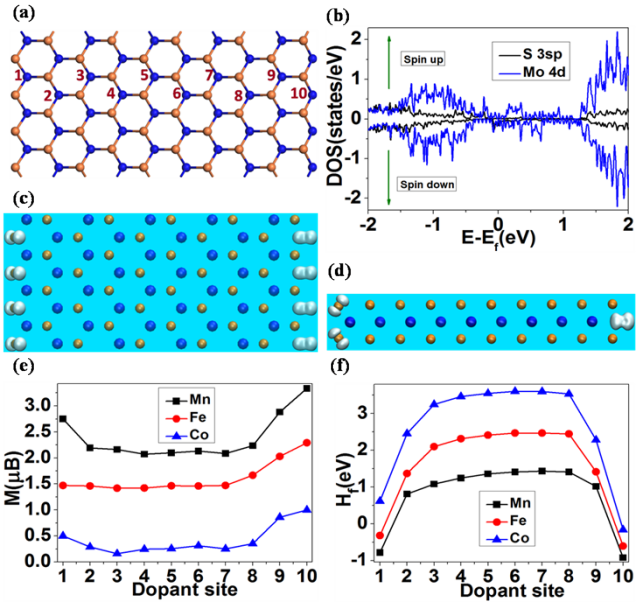

Fig. 3 (a) Top view of the geometric structure of relaxed 10-$ZMoS_2$NR and its ten substitutional sites. (b) SPDOS of 10-$ZMoS_2$NR. (c) Top and (d) side views of the 0.02 e/Å^3 isosurface of the magnetization density distribution of the 10-$ZMoS_2$NR. Configuration-dependent (e) formation energy and (f) M of 3d TM impurities of doped 10-$ZMoS_2$NRs.

The electronic and magnetic properties of zigzag MoS_2 nanoribbons ($ZMoS_2$NRs) doped with 3d TMs were also

investigated. The relaxed structure of clean 10-ZMoS$_2$NR is shown in Fig. 3(a). From the SPDOS (Fig. 3(b)), 10-ZMoS$_2$NR shows spontaneous magnetization. The Mo 4d shows strong spin-polarization whereas the S 3sp is weakly spin-polarized. The band gap of both majority and minority bands is zero. Thus 10-ZMoS$_2$NR is a metallic magnet. Each outermost Mo has the strongest magnetization, with a local magnetic moment of 0.7 μ_B whereas each outermost S has a local magnetic moment of 0.3 μ_B. The magnetization is mainly localized on the edges of 10-ZMoS$_2$NR (see Fig. 3(c) and (d)).

3d TM impurities are used to dope the 10-ZMoS$_2$NR to modulate the electronic and magnetic properties. Ten substitutional sites of 3d TM dopant with a concentration of 2.5 percent are considered for the 10-ZMoS$_2$NR (Fig. 3(a)). The width of the relaxed 10-ZMoS$_2$NR is around 2.6 nm. The stabilities of the configurations are analyzed by comparing the formation energies of different configurations (see Fig. 3(e)). For Mn-, Fe-, and Co-doped 10-ZMoS$_2$NRs, configuration 10 has the lowest formation energy because the bonds between the impurities and host atoms can be fully relaxed at the edges. Configuration 1 has the second lowest formation energy. Configuration 6 has the largest formation energy because the relaxation of the bonds between impurities and host atoms are restricted. This can be interpreted as an edge effect in which the formation energy is lower the nearer the impurities are to the edge. This is in agreement with experimental scanning transmission electron microscopy (STEM) findings that Co impurities replace the cations at the Mo edges of MoS$_2$ nanowires.[11] Although there is rarely experimental reports on the substitutional behaviors of Mn and Fe of Mo in MoS$_2$, from a thermodynamic point of view, we predict that Mn and Fe will also replace the cations at the Mo edges of MoS$_2$.

From Fig. 3(f), the 3d TM impurities of configuration 10 have the largest magnetic moment with Mn, Fe, and Co having local magnetic moments of 3.3, 2.4, and 1.0 μ_B, respectively. Similarly, Mn, Fe, and Co adatoms on the MoS$_2$ monolayer have local magnetic moments of 3.0, 2.0, and 1.0 μ_B, respectively.[22] Impurities of the 3d TM-doped 10-ZMoS$_2$NRs exhibit obvious configuration-dependent magnetic properties. The nearer the impurities are to the edge, the larger the magnetic moments are.

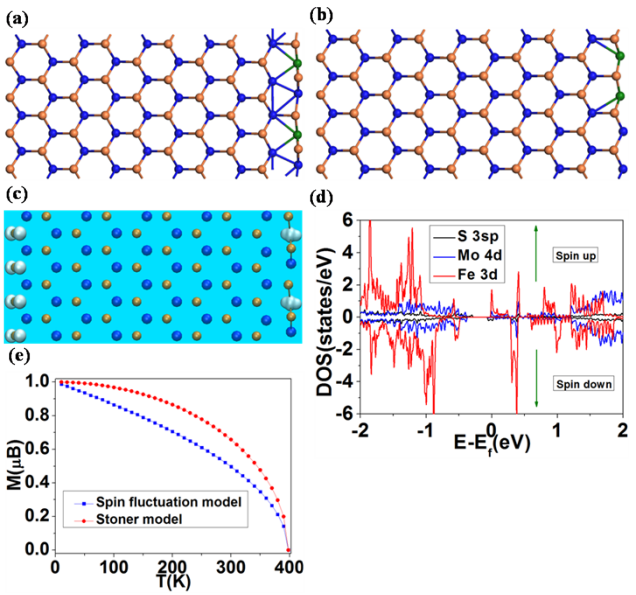

Fig. 4 Top views of Fe-impurity-pair-doped 10-ZMoS$_2$NRs with configuration (a) γ and (b) δ. (c) 0.02 e/Å^3 isosurface and (d) SPDOS of the FM state of configuration γ. (e) Temperature-dependent *M* of Co impurity in doped 10-ZMoS$_2$NR with configuration γ.

To investigate the magnetic exchange coupling between impurities, we increased the dopant concentration to 5 percent. For the calculated structures of 10-ZMoS$_2$NR doped with Co-impurity pairs (Fig. 4(a) and (b)), the total energy of configuration γ is 0.16 eV smaller than that of configuration δ; thus configuration γ is more stable than configuration δ. Co impurities are distributed uniformly at the Mo edge. For Mn- and Fe-doped 10-ZMoS$_2$NRs, the total energy of configuration γ is 0.11 and 0.03 eV respectively smaller than that of configuration δ, and hence Mn and Fe are also distributed uniformly at the Mo edge. For Co-doped 10-ZMoS$_2$NRs with configuration γ, there is strong structural reconstruction at the Mo edge (Fig. 4(a)). Co atoms are relaxed towards interior sites of 10-ZMoS$_2$NR and form bonds with neighboring Mo atoms, and thereby stabilize this configuration γ. From experimental STEM images, configuration γ appears for Co-doped WS$_2$ nanowires.[11]

Table 2 Summary of Δ*E* (meV) for 3d TM impurity-doped ZMoS$_2$NRs with different widths. γ and δ indicate the configurations γ and δ, respectively

	6_γ	6_δ	8_γ	8_δ	10_γ	10_δ	12_γ	12_δ
Mn	76	-86	103	-88	115	-79	107	-83
Fe	30	28	32	35	26	48	23	51
Co	74	66	78	70	69	71	73	75

From Table 2, ΔE is 68 and 71 meV for the configurations γ and δ, respectively, of Co-doped 10-$ZMoS_2$NRs. Each Co impurity has a magnetic moment of 1.0 μ_B; thus we can take $S=S_1=S_2=0.5$ here. According to $J=\Delta E/(4S_1 \cdot S_2)$, the magnetic exchange coupling is 69 and 71 meV for configurations γ and δ, respectively. The corresponding T_C is 398 and 410 K calculated by eqn (4). Thus Co-doped 10-$ZMoS_2$NR manifests a strong FM nature with T_C above room temperature. The magnetization distribution of Co-doped 10-$ZMoS_2$NRs with configuration γ. Fig. 4(c) shows the magnetization is mainly distributed on the edgiest S and Co atoms. Each edgiest S has a local magnetic moment of 0.4 μ_B, which is 0.1 μ_B larger than that of clean 10-$ZMoS_2$NR. Thus doping the right Mo edge with Co impurities could also influence the magnetic properties of the left S edge of 10-$ZMoS_2$NR. These two edges contribute mainly to the states near the Fermi level and dominate the physical properties of 10-$ZMoS_2$NRs.

The DOS of the FM state for Co-doped 10-$ZMoS_2$NR with configuration γ (Fig. 4(d)) shows the Co impurities exhibit strong spin-polarization. For both spin-up and spin-down bands, the electrons occupy the Fermi-level states. Co-doped 10-$ZMoS_2$NR is still metallic, but the DOS distribution near the Fermi level has been strongly tuned by impurities in contrast to clean 10-$ZMoS_2$NR. The temperature-dependent magnetic moment of Co-doped 10-$ZMoS_2$NR (Fig. 4(e)) shows that as the temperature increases, the magnetic moment decreases. At room temperature, the magnetic moment of the Co-impurity is 0.5 and 0.7 μ_B, predicted by spin-fluctuation and Stoner models, respectively. From Table 2, ΔE is positive for Co-doped 6-, 8-, and 12-$ZMoS_2$NRs, so these $ZMoS_2$NRs also possess an FM ground state. According to eqn (4), the T_Cs of these Co-doped $ZMoS_2$NRs are also above room temperature.

Also from Table 2, Mn-doped $ZMoS_2$NRs exhibit configuration-dependent magnetic properties. Configuration γ is FM, whereas configuration δ is AFM. For Mn-doped 10-$ZMoS_2$NR, we can take $S=S_1=S_2=1.65$, because each Mn has a local magnetic moment of 3.3 μ_B. In accordance with $J=\Delta E/(4S_1 \cdot S_2)$, the magnetic exchange coupling is 10.9 and −7.3 meV for configurations γ and δ, respectively. The T_C is 355 K for configuration γ calculated by eqn (4). For Mn-doped $ZMoS_2$NRs, configuration δ exhibits AFM characteristics due to the superexchange interaction between the nearest-neighbor Mn atoms, while in configuration γ the impurities are remote. Similar effects were also found for Mn doped ZnO with impurities in the nearest-neighboring configuration.[28, 29]

All Fe-doped $ZMoS_2$NRs exhibit FM characteristics. Regarding Fe-doped 10-$ZMoS_2$NRs, we can take $S=S_1=S_2=1.2$ here as each Fe has a local magnetic moment of 2.4 μ_B. From $J=\Delta E/(4S_1 \cdot S_2)$, the magnetic exchange coupling is 4.5 and 8.3 meV for configurations γ and δ, respectively, with corresponding T_C of 91 and 169 K. Again, the T_Cs are well below room temperature, thus Fe-doped 10-$ZMoS_2$NRs manifest weak FM characteristics. Although $ZMoS_2$NRs are natural magnetic, incorporating 3d TM impurities could further tune their magnetic and electronic properties.

Conclusions

In summary, the electronic and magnetic properties of MoS_2 nanoribbons can be tuned with 3d TM impurities. These impurities tend to substitute the edgiest cations of $AMoS_2$NRs and $ZMoS_2$NRs. Fe-doped $AMoS_2$NRs manifest a FM semiconductor nature and their T_C can be tuned by adding impurities. In contrast, Co and Mn-doped $AMoS_2$NRs are AFM semiconductors. Co-doped $ZMoS_2$NRs show metallic and strong FM characteristics with T_C above room temperature. Mn-doped $ZMoS_2$NRs show configuration-dependent magnetic properties. Fe-doped $ZMoS_2$NRs are weak FM semiconductors. Our results provide an insight at the atomic level of the electronic and magnetic properties of 3d TM-doped MoS_2 nanoribbons and pave the way for future applications of MoS_2 and other transition metal dichalcogenides in nanoelectronic and spintronic devices.

Acknowledgements

The author gratefully acknowledges financial support from National Natural Science Foundation of China (Nos. 11304206 and 21001051), National Natural Science Foundation of Shenzhen University (Nos. 827000001 and 82700002601) and Strategic Emerging Industry Development Special Fund of Shenzhen (JCYJ20130326111743703 and JC201105170651A) and Shenzhen Key Laboratory of Sensor Technology Open Project (SST201302) and Shenzhen Key Laboratory of Special Functional Materials Open Project (T201303). The authors would thank the National Supercomputing Center in Shenzhen and the High Performance Computing Center of Shenzhen University for the computational facilities.

Notes and references

[a] College of Physics and Technology and Shenzhen Key Laboratory of Sensor Technology, Shenzhen University, Shenzhen 518060, Guangdong, P. R. China. E-mail: duyu@szu.edu.cn

[b] Department of Mechanical Engineering and Materials Science, Department of Chemistry, and the Smalley Institute for Nanoscale Science and Technology, Rice University, Houston, Texas 77005, United States. E-mail: biy@rice.edu

[c] Department of Electronic Engineering and Materials Science and Technology Research Center, The Chinese University of Hong Kong, Shatin, N.T., Hong Kong SAR, People's Republic of China

1 K. F. Mak, C. Lee, J. Hone, J. Shan, and T. F. Heinz, *Phys. Rev. Lett.*, 2010, **105**, 136805.

2 V. V. Ivanovskaya, A. Zobelli, A. Gloter, N. Brun, V. Serin, and C. Colliex, *Phys. Rev. B.*, 2008, **78**, 134104.

3 M. Remskar, A. Mrzel, M. Virsek, M. Godec, M. Krause, A. Kolitsch, A. Singh, and A. Seabaugh, *Nanoscale Res. Lett.*, 2011, **6**, 26.

4 Z. Y. Wang, H. Li, Z. Liu, Z. J. Shi, J. Lu, K. Z. Suenaga, S.-K. Joung, T. Okazaki, N. Gu, J. Zhou, Z. X. Gao, G. P. Li, S. Sanvito, E. G. Wang, and S.Iijima, *J. Am. Chem. Soc.*, 2010, **132**, 13840.

5 Li, Y. F. Zhou, Z. Zhang, S. B. Chen, and Z. F. Chen, *J. Am. Chem. Soc.*, 2008, **130**, 1673.

6 C. Ataca, H. Sahin, E. Akt€urk, and S. Ciraci, *J. Phys. Chem. C*, 2011, **115**, 3934.

7 H. Qiu, T. Xu,. Z. L. Wang, W. Ren, H. Y. Nan, Z. H. Ni, Q. Chen, S. J. Yuan, F. Miao, F. Q. Song, G Long, Y. Shi, L. T. Sun, J. L. Wang, and X. R. Wang, *Nat. Commun.*, 2013, **4**, 2642.

8 X. L. Zou, Y. Y. Liu, and B. I. Yakobson, Nano Lett., 2013, 13, 253.

9 H. L. Shi, H. Pan, Y. W. Zhang, and B. I. Yakobson, *Phys. Rev. B*, 2013, **87**, 155304.

10 L.Z. Kou, C. Tang,Y Zhang,T. Heine,C. F. Chen, and T. Frauenheim, J. *Phys. Chem. Lett.* 2012, **3**, 2934.

11 F. L. Deepak, R. Esparza, B. Borges, X. L. Lozano, and M. J. Yacaman, *ACS Catal.*, 2011, **1**, 537.

12 G. Leyral, M. Ribes, L. Courthéoux, D. Uzio, and A. Pradel, *Eur. J. Inorg. Chem.*, 2012, **31**, 4967.

13 I. Popov, G. Seifert, and D. Toma´nek, *Phys. Rev. Lett.*, 2012, **108**, 156802.

14 X. Huang, Z.Y. Zeng, S.Y. Bao, M.F. Wang, X.Y. Qi, Z.X. Fan, and H. Zhang, *Nat. Commun.*, 2013, **4**, 1444 ().

15 P. Giannozzi, S. Baroni, N. Bonini, M. Calandra, R. Car, C. Cavazzoni, D. Ceresoli, Chiarotti, G. L. Cococcioni, M. Dabo, I. Dal Corso, A. de Gironcoli, S. Fabris, S. Fratesi, G. Gebauer, and R. Gerstmann, U., et al. *J. Phys. Condens. Matter*, 2009, **21**, 395502-395520.

16 J. P. Perdew, Burke, and K. Ernzerhof, M. *Phys. Rev. Lett.*, 1996, **77**, 3865.

17 S. L. Dudarev, G. A. Botton, S. Y. Savrasov, C. J. Humphreys, and A. P. Sutton, *Phys. Rev. B*, 1998, **57**, 1505.

18 S. K. Nayak., *A treatise on First-principles Studies of ZnO as Diluted Magnetic Semiconductor*, Doctoral Thesis, University of Duisburg-Essen, 2012.

19 J.-M. Zhang, W.G. Zhu, Y. Zhang, D. Xiao, and Y. G. Yao, *Phys. Rev. Lett.*, 2012, **109**, 266405.

20 W. Tang, E. Sanville, and G. Henkelman, *J. Phys.: Condens. Matter* 2009, **21**,084204.

21 Kapildeb Dolui, Chaitanya Das Pemmaraju, and Stefano Sanvito, *ACS Nano*, 2012, **6**, 4823-4834.

22 C. Ataca and S. Ciraci, *J. Phys. Chem. C* 2011, **115**, 13303

23 T. Zhang, L. X. Song, Z. Z. Chen, E.-W. Shi, L.X. Chao, and H. W. Zhang, *Appl. Rev. Lett.*, 2006, **89**, 172502.

24 C. Kittel: *Introduction to Solid State Physics, 8th Edition* (John Wiley & Sons, Inc., New York Chichester Brisbane Singapore Toronto, **2005**).

25 C. F. Hirjibehedin, C.-Y. Lin, A. F. Otte, M. Ternes, C. P. Lutz, B. A. Jones, and A. J. Heinrich, *Science*,2007, **317**,1199.

26 P. Mohn,: *Magnetism in the Solid State: An Introduction (Springer-Verlag*, Berlin Heidelberg, **2006**).

27 M. Ferhat, A. Zaoui, and R. Ahuja, *Appl. Phys. Lett.*, 2009, **94**, 142502.

28 S. Basu, D. Y. Inamdar, Shailaja Mahamuni, Aparna Chakrabarti, C. Kamal, G. Ravi Kumar,S. N. Jha,and D. Bhattacharyya, *J. Phys. Chem. C* 2014, **118**, 9154.

29 M. H. F. Sluiter, Y. Kawazoe, P. Sharma, A. Inoue, A. R. Raju, C. Rout, and U.V. Waghmare, *Phys. Rev. Lett.* 2005, **94**, 187204.